JOURNAL
COMPUTER SCIENCES INSTITUTE

JCSI 37 (2025) 410–417
Received: 17 June 2025
Accepted: 12 November 2025

Comparative analysis of methods for identifying tree structures of coronary vessels

Analiza porównawcza metod identyfikacji struktur drzewiastych naczyń wieńcowych

Kacper Miłosz Liżewski*, Małgorzata Charytanowicz

Department of Computer Science, Lublin University of Technology, Nadbystrzycka 36B, 20-618 Lublin, Poland

Abstract
The paper presents a comparative analysis of the performance of machine learning models and one filter method used for semantic segmentation of the coronary vessels based on the source coronary angiographic image. Seven machine learning models were tested: UNet3+, AngioNet, Reg-SA-UNet++, EfficientUNet++ B5, SE-RegUNet 4GF, SE-RegUNet 16GF, FR-UNet and one filter method, which was implemented as part of the paper. Despite the impossibility of determining the exact hierarchy of model performance, based on the results of statistical tests, the model that presented the best results with accuracy of 97,7% was distinguished – FR-UNet and the model that showed the lowest quality – UNet3+.

Keywords: coronary angiography; image segmentation; machine learning

Streszczenie
W pracy zaprezentowano analizę porównawczą jakości działania modeli uczenia maszynowego oraz jednej metody filtrowej służących do segmentacji semantycznej struktury ukrwienia wieńcowego na podstawie źródłowego obrazu koronarograficznego. Badaniu poddano siedem modeli uczenia maszynowego: UNet3+, AngioNet, Reg-SA-UNet++, EfficientUNet++ B5, SE-RegUNet 4GF, SE-RegUNet 16GF, FR-UNet oraz jedną metodę filtrową, która została zaimplementowana w ramach pracy. Pomimo braku możliwości wyznaczenia dokładnej hierarchii działania modeli, na podstawie wyników testów statystycznych, został wyodrębniony model, który prezentował najlepsze wyniki i osiągnął dokładność 97,7% – FR-UNet oraz model, który wykazał najniższą jakość – UNet3+.

Słowa kluczowe: koronarografia; segmentacja obrazów; uczenie maszynowe

*Corresponding author
Email address: s95480@pollub.edu.pl (K. M. Liżewski)

1. Introduction

Coronary artery disease is one of the leading causes of death worldwide. According to statistics from the World Health Organization (WHO) in 2021 it accounted for 13% of all deaths worldwide with the highest risk group being citizens of high- and middle-income countries [1]. The reduction of the lumen of the arteries or their complete occlusion impairs the blood supply to the heart, and consequently an insufficient supply of oxygen. Untreated coronary artery disease leads to coronary insufficiency, angina pectoris and myocardial infarction and most often ends in the death of the patient.

The growing popularity and development of machine learning and artificial intelligence methods have resulted in great interest among scientists in research on the creation of diagnostic tools that allow for the detection of anomalies in the geometric tree structure of coronary vessels, even at the early stage of development of coronary diseases.

Historically, filter methods using the Hessian filter [2], Hough transform and directed filter [3], local energy function [4], ROI area of interest with mathematical theory of flux flow [5] and graph theory [6] are known to solve this problem.

In the context of machine learning, the U-Net architecture [7] is widely used in the process of semantic segmentation of coronary vessels. The UNet 3+ [8] architecture introduced a new way of combining features from different levels of the network and deep supervision was applied. As part of the research on the UNet++ architecture [9], it was shown that the use of shortcut paths in the network reduced the loss of semantic information between the feature maps of the encoder and decoder structure. The FR-UNet network [10] is characterized by preserving full resolution information in the process of signal propagation through the network. The analysis also included the possibility of using residual blocks [11], used to construct the Reg-SA-UNet++ [12] or SE-RegUNet [13] networks. The DeepLabV3+ architecture was also used for the task of semantic segmentation of coronary vessels, on the basis of which the AngioNet network [14] was built. Many authors have drawn attention to the significant improvement in prediction efficiency through the use of image preprocessing stages, which highlighted features important from the point of view of semantic segmentation [5, 13, 14].

The aim of this work is to conduct a comparative analysis of methods for semantic segmentation of coronary vessels based on source coronary angiography. Seven machine learning methods and one filter method, which was implemented in the research based on the article [5] were analyzed. All methods were evaluated on one set of coronary angiography image pairs and their labels. The results were subjected to statistical tests to determine the hierarchy of the performance quality of models and methods.

2. Research material

The evaluation dataset used to conduct the experiment is the publicly available DCA1 (Database X-ray Coronary Angiograms) [15]. The DCA1 database consists of 134 coronary angiographic images with ground truths that were manually created by domain experts in cardiology. Each pair of grayscale images has dimensions of 300×300 pixels and is saved in the PGM (Portable Gray Map) format.

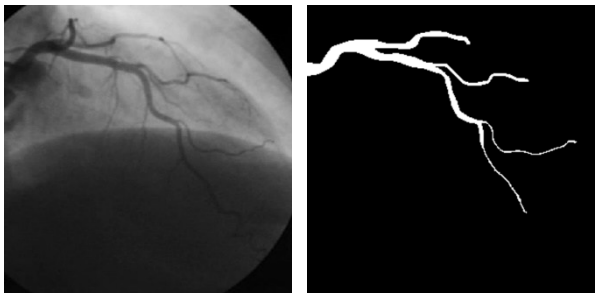

(a) (b)

Figure 1: Single images pair from DCA1. Source coronary angiography (a) and its corresponding segmentation mask (b).

DCA1 is a set dedicated to the study of the performance of semantic segmentation methods for coronary vessels and in the context of the study covered by this work it will constitute one coherent set, providing comparative objectivity for selected machine learning models and algorithms. Figure 1 shows an example pair of images selected from the DCA1 dataset [15].

3. Selected models

The research experiment carried out for the purposes of this work will be performed using the following machine learning models and the implementation of segmentation method based on the detection of the area of interest (ROI) and the flux-flow measure [5]:

- AngioNet (M1) [14],
- Modified UNet3+ architecture (M2) [16],
- EfficientUNet++ B5 (M3) [17],
- Reg-SA-UNet++ (M4) [12],
- FR-UNet (M5) [10],
- SE-RegUNet 16GF (M6) [13],
- SE-RegUNet 4GF (M7) [13],
- Own implementation of the filter method (M8) [5].

3.1. AngioNet

The AngioNet network consists of two smaller neural networks, the first of which is responsible for predicting the best possible kernel in the convolution operation, so as to perform the initial processing of the digital image as efficiently as possible, while the second is responsible for performing the actual semantic segmentation process. The image is processed sequentially.

The coronary angiography processing neural network (APN) receives as input a 512×512 pixel grayscale coronary angiography, subjected to the standardization process, while the result of the APN inference is a single-channel digital image.

The next stage is the concatenation of the single-channel digital image and the original X-ray image, thanks to which an image containing three channels is placed at the input to the DeepLabV3+ basic segmentation model with the Xception skeleton and the actual segmentation mask prediction process is performed.

3.2. Modified UNet3+ architecture

Compared to the reference U-Net 3+ architecture, the authors have introduced a modification of the encoder architecture, which is based on residual and inception modules. The blocks are designed to capture multidimensional features to improve segmentation accuracy. The method uses full-dimensional deep supervision. Weights of the neural network are optimized in this solution by comparing the differences between the ground truth and the intermediate network results. Finally, Otsu's thresholding algorithm was used to transform the probability map into a binary segmentation mask.

3.3. EfficientUNet++ B5

The network consists of encoder layers, which extract features from a digital image, and then the decoder, based on the extracted features, recreates a digital image of the same size as the image that is the input signal to the process. The improvement introduced was the concept of using an EfficientNet-B5 encoder layer and an EfficientUNet++ decoder in the basic U-Net++ architecture. The modifications introduced consist in replacing the convolution layer with a 3×3 kernel size with residual blocks using deep convolutions and applying a channel and spatial attention mechanism to feature maps using concurrent scSE blocks. The rest of the U-Net++ architecture remains unchanged in this solution.

3.4. Reg-SA-UNet++

The Reg-SA-UNet++ model is a modified UNet++ architecture and its main improvement is the enhancement of feature extraction. The changes introduced in the network encoder layer consisted in using the RegNet block developed as part of the research work of the Facebook AI Research group, as the basic encoder block, which reduces the number of neural network parameters and increases the possibilities of feature extraction.

3.5. FR-UNet

The FR-UNet network is a modification of the basic UNet++ architecture. The deep connections present in each phase of the network were removed, and in their place a multiresolution interactive convolution mechanism was applied. The shallow phase provides more semantic information, while the deep phases complement high-level context information and increase the local receptive fields of the feature map. In order to reduce the parameters of the neural network, feature maps were combined only and exclusively between neighboring phases, which increased the diversity and efficiency of feature aggregation. The parallel process of aggregating feature maps from congruent nodes allows the network to learn hierarchical representations. In contrast to classical solutions based on the encoder-decoder architecture, the first phase of the network continuously integrates high-level context information while maintaining the original resolution.

3.6. SE-RegUNet

The concept of the SE-RegUNet segmentation model uses a pre-processing step in the process to achieve better prediction results of the deep convolutional network by normalizing the contrast and enhancing the edge sharpness of the coronary angiography image at the model input. The pre-processing step combines two well-established digital image processing methods: USM and CLAHE. The basic concept of the new convolutional network architecture is to replace the encoder layer with the RegNet structure developed by the Facebook AI Research group. The SE-RegUNet network is therefore a fusion of the U-Net and RegNet convolutional neural networks.

3.7. Filter method

The proposed classical method of coronary vessel segmentation consists of several stages. The first stage in the process is the pre-processing of the coronary angiographic image in order to highlight its expected features using the USM filter. After the pre-processing stage, the process is divided into two independent paths - ROI detection and application of the flux flow in digital image processing, combined with Otsu thresholding. The result of this connection is a binary flux flow mask. In the decision step, in which the ROI detection and Otsu thresholding stages are combined, a decision is made to match the appropriate semantic category. In the last step of algorithm processing, mask cleaning procedures were performed.

4. Experiment

This chapter presents the experimental procedures conducted to investigate the proposed hypotheses. It outlines the design, methodology, and tools used in the experiments, as well as the conditions under which they were performed. The goal is to ensure transparency and reproducibility of the results discussed in subsequent sections.

4.1. Transformation of two-dimensional signals

All considered machine learning models and algorithms process digital images in the size of 512×512 pixels. Due to the fact that the original data from the DCA1 set are digital images with the size of 300×300 pixels, these two-dimensional signals should be transformed without significant loss of information. For this purpose, the OpenCV library [18] was used.

In order to perform further studies, it is necessary to confirm that there is no significant difference between the original two-dimensional signals and the transformed signals, which will confirm the validity of further studies. For this purpose, the average value of the Structural Similarity Index Measure (SSIM) [19] was calculated for all pairs of coronary angiographic images and their labels in the original and transformed versions, which is used to measure the similarity of pairs of digital images.

The SSIM can take values from the range $[-1,1]$, where the value 1 indicates perfect similarity, 0 – no similarity, and -1 corresponds to perfect anti-correlation. The procedure for calculating the metric value was called for two sets – coronary angiography and their labels, where $SSIM_I = 0.9985$ for coronary angiography pairs and $SSIM_L = 0.8661$ for segmentation mask pairs were obtained. These results indicate a high similarity of the transformed and source signals.

4.2. Method

The selected models and algorithms will be evaluated on the DCA1 dataset. For this purpose, inference will be performed by each of the models and algorithms, the result of which will be segmentation masks. Then, based on the reference and inferred masks, the values of the evaluation metrics will be calculated. The evaluation criteria will be the following metrics:

- Accuracy (ACC)
- Precision (PRE)
- Sensitivity (SENS)
- Specificity (SPEC)
- Intersection over Union (IoU)
- Dice Score (DSC, F1)

The study will be conducted based on trained model weights. For the FR-UNet model, the trained weights were taken from the official model repository on the GitHub platform [20], while for the AngioNet, UNet3+, EfficientUNet++ B5, Reg-SA-UNet++ and SE-RegUNet (4/16GF) models were taken from the repository on the Hugging Face platform [21], which was created as part of the research [13].

The raw results will be subjected to statistical tests that will allow for the construction of a hierarchy of model quality. Accordingly, the Friedman rank test [22] will be performed for each considered evaluation metric to determine whether there is a significant statistical difference between the models, and the Nemenyi post-hoc tests [23], which are designed to find specific groups of data that differ from each other.

5. Results

This section presents the outcomes of the conducted experiments and analyses aimed at evaluating the performance of the considered methods. The results enable a comparison of the approaches based on selected evaluation metrics and highlight statistically significant differences between models.

Table 1 – Table 6 present descriptive statistics for each metric considered, which include the mean, standard deviation, median, first and third quartiles. Each sample size was 134 observations for a single model The models are described in the tables by aliases included in Section 3 of this work.

Table 1 Descriptive statistics for ACC metric

Model	Mean	SD	Md	Q1	Q3
M1	0.948	0.023	0.955	0.943	0.963
M2	0.955	0.010	0.957	0.949	0.964
M3	0.942	0.014	0.943	0.933	0.951
M4	0.943	0.022	0.950	0.933	0.958
M5	**0.977**	**0.006**	**0.978**	**0.973**	**0.982**
M6	0.958	0.010	0.959	0.953	0.966
M7	0.949	0.029	0.959	0.937	0.968
M8	0.880	0.055	0.880	0.840	0.924

Table 2 Descriptive statistics for PRE metric

Model	Mean	SD	Md	Q1	Q3
M1	0.684	0.152	0.714	0.573	0.800
M2	0.784	0.117	0.795	0.728	0.876
M3	0.422	0.109	0.433	0.355	0.484
M4	0.787	0.125	0.807	0.736	0.880
M5	**0.797**	**0.068**	**0.798**	**0.760**	**0.843**
M6	0.767	0.103	0.760	0.699	0.858
M7	0.764	0.146	0.792	0.672	0.876
M8	0.437	0.226	0.453	0.260	0.609

Table 3 Descriptive statistics for SENS metric

Model	Mean	SD	Md	Q1	Q3
M1	0.546	0.126	0.564	0.467	0.628
M2	0.562	0.085	0.568	0.524	0.608
M3	0.189	0.083	0.170	0.134	0.247
M4	0.495	0.129	0.507	0.411	0.573
M5	**0.777**	**0.082**	**0.795**	**0.738**	**0.838**
M6	0.592	0.090	0.590	0.548	0.640
M7	0.560	0.164	0.585	0.457	0.675
M8	0.265	0.214	0.198	0.091	0.403

Table 4 Descriptive statistics for SPEC metric

Model	Mean	SD	Md	Q1	Q3
M1	0.981	0.011	0.984	0.976	0.989
M2	0.987	0.009	0.989	0.983	0.993
M3	0.986	0.005	0.986	0.982	0.990
M4	0.987	0.009	0.989	0.985	0.993
M5	**0.989**	**0.005**	**0.989**	**0.986**	**0.992**
M6	0.986	0.009	0.986	0.982	0.992
M7	0.986	0.011	0.989	0.981	0.993
M8	0.966	0.016	0.967	0.958	0.978

Table 5 Descriptive statistics for IoU metric

Model	Mean	SD	Md	Q1	Q3
M1	0.427	0.108	0.433	0.344	0.510
M2	0.484	0.084	0.492	0.442	0.540
M3	0.147	0.058	0.145	0.101	0.192
M4	0.438	0.117	0.459	0.360	0.526
M5	**0.644**	**0.060**	**0.651**	**0.611**	**0.683**
M6	0.496	0.071	0.496	0.448	0.550
M7	0.470	0.137	0.497	0.364	0.585
M8	0.201	0.156	0.143	0.075	0.301

Table 6 Descriptive statistics for DSC metric

Model	Mean	SD	Md	Q1	Q3
M1	0.591	0.109	0.605	0.511	0.675
M2	0.648	0.080	0.660	0.613	0.701
M3	0.252	0.089	0.253	0.183	0.322
M4	0.600	0.121	0.629	0.530	0.690
M5	**0.782**	**0.046**	**0.788**	**0.758**	**0.812**
M6	0.660	0.066	0.664	0.619	0.710
M7	0.627	0.137	0.664	0.534	0.738
M8	0.308	0.205	0.250	0.140	0.462

The analysis began with the Friedman rank test applied to each of the considered metrics, following the stated hypotheses:

H_0 – *the performance of the models with respect to the metric* M *is the same*

H_A – *the performance of the models with respect to the metric M differs significantly*

We assume the level of statistical significance of $\alpha = 0.05$. Table 7 presents the test results for each selected metric.

Table 7: Friedman rank test for all selected metrics

Evaluation metric (M)	χ^2(df=7) statistic	p-value
ACC	547.3856	$p < 0.001$
PRE	513.2562	$p < 0.001$
SENS	616.5348	$p < 0.001$
SPEC	320.0622	$p < 0.001$
IoU	686.4677	$p < 0.001$
DSC	686.4677	$p < 0.001$

The Friedman rank test revealed statistically significant differences between the evaluated models. This indicates that the models do not perform equally across the considered metrics.

Since the test for each metric showed a significant statistical difference, Nemenyi post-hoc tests were performed for each metric to determine which groups of data differ significantly from each other. The results of Nemenyi tests are presented in Figure 2 – Figure 7 as heatmaps with four significance levels at which the models differ from each other, i.e. 0.05, 0.01, 0.001 and no statistically significant differences, respectively.

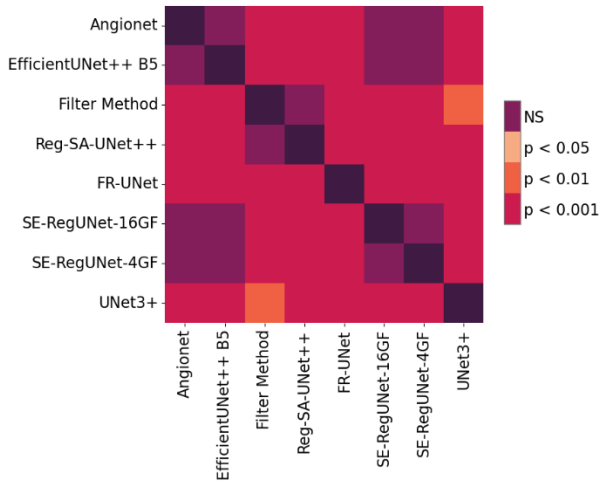

Figure 2: Heatmap of p-values for ACC metric based on Nemenyi post-hoc test.

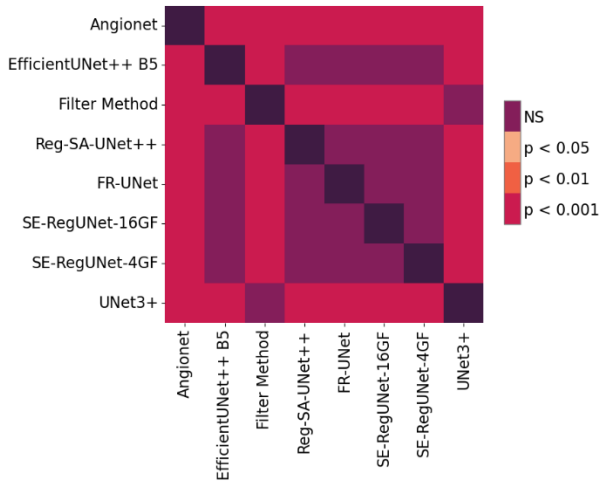

Figure 3: Heatmap of p-values for PRE metric based on Nemenyi post-hoc test.

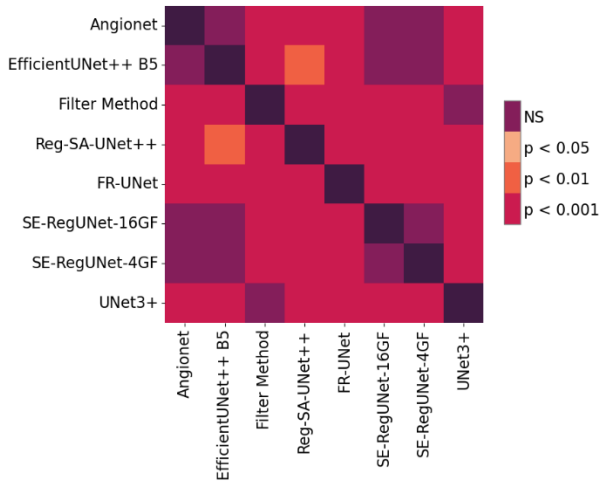

Figure 4: Heatmap of p-values for SENS metric based on Nemenyi post-hoc test.

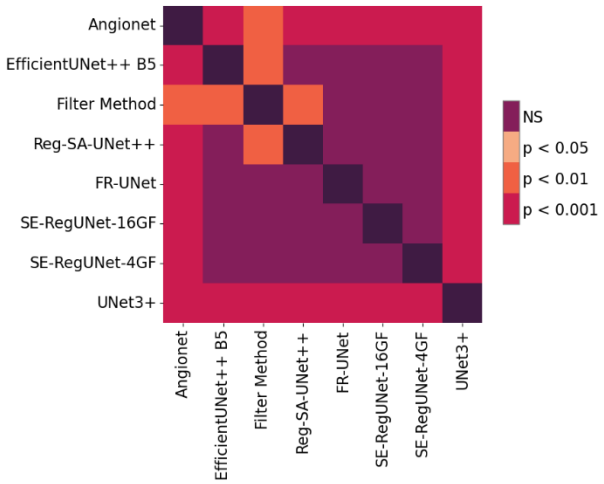

Figure 5: Heatmap of p-values for SPEC metric based on Nemenyi post-hoc test.

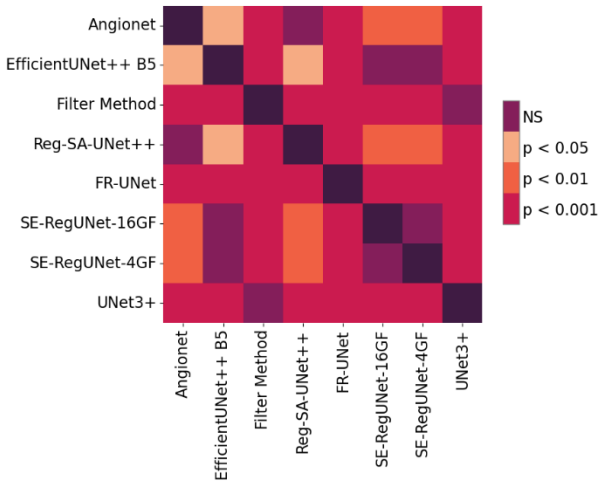

Figure 6: Heatmap of p-values for IoU metric based on Nemenyi post-hoc test.

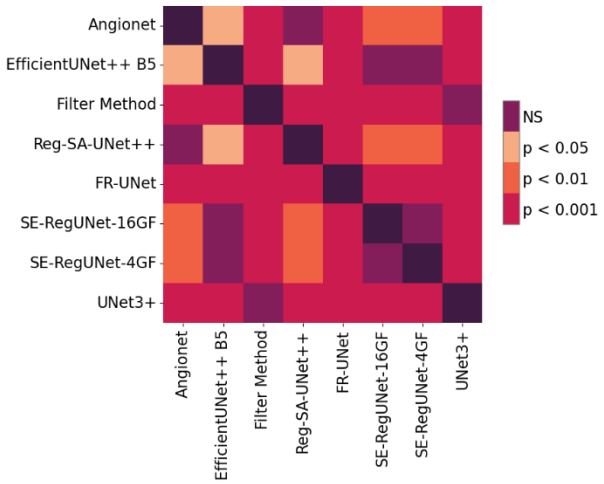

Figure 7: Heatmap of p-values for DSC metric based on Nemenyi post-hoc test.

Critical difference diagrams help interpret results for individual metrics. Model ranks were assigned based on average values. Figure 8 presents the averaged metric values for each model.

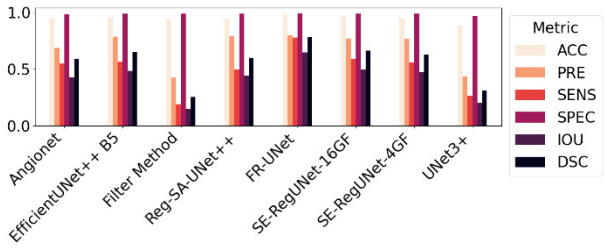

Figure 8: Average metrics values for each model considered.

Figure 9 shows that for the accuracy metric we can distinguish four groups of models that differ significantly from each other. UNet3+ showed the worst results. The filter method and the Reg-SA-UNet++ network are the next group of methods showing better results than the UNet3+ network, but worse than the group consisting of the models: AngioNet, EfficientUNet++ B5, SE-RegUNet 4GF, SE-RegUNet 16GF. The best results were presented by the FR-UNet model.

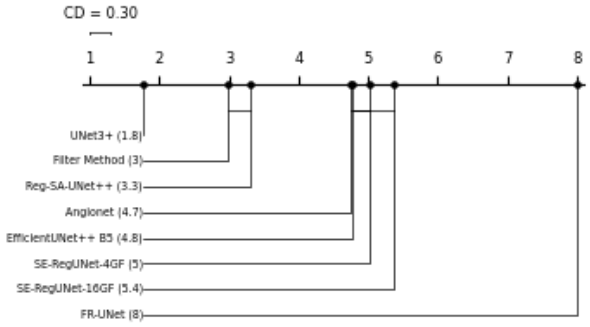

Figure 9: Critical difference diagram for all considered models for the ACC metric.

Considering the precision metric (Figure 10), the models were divided into three groups of equivalent methods, which presented very similar results. The group of methods that showed the worst results consists of the filter method and the UNet3+ network. The next group consisted of only one AngioNet model, while the rest of the considered models did not show significant differences considering the precision.

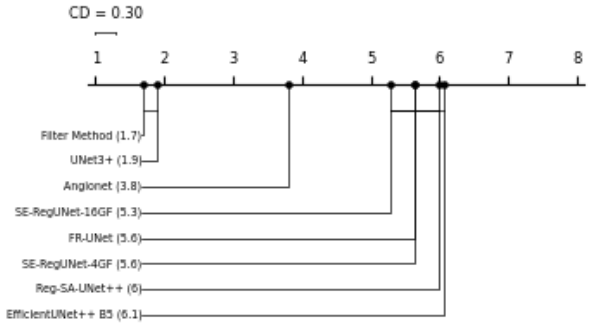

Figure 10: Critical difference diagram for all considered models for the PRE metric.

Considering the sensitivity metric (Figure 11), the models are divided into four groups presenting identical quality. The worst results were presented by the group consisting of the UNet3+ model and the filter method. The next group showing better results was the single-element group with the Reg-SA-UNet++ model. The third and the most numerous group presented clearly better results than the Reg-SA-UNet++ network, while the FR-UNet network undoubtedly presented the best results.

For the specificity metric (Figure 12), three groups of models were clearly formed showing identical results, while the last group, presenting the best results, is not uniform. It would be possible to build its internal hierarchy, but in view of the other results, this is unnecessary. The UNet3+ network showed the worst results, while the AngioNet network was placed between the groups with the worst and the best results, building a single-element central group.

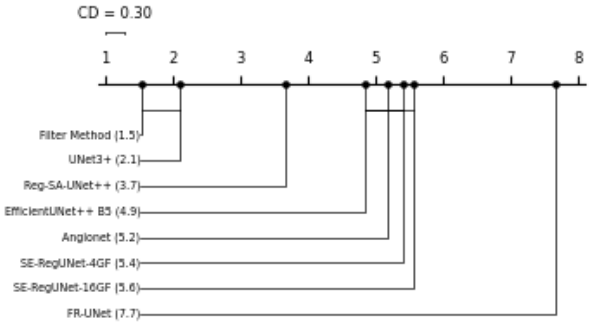

Figure 11: Critical difference diagram for all considered models for the SENS metric.

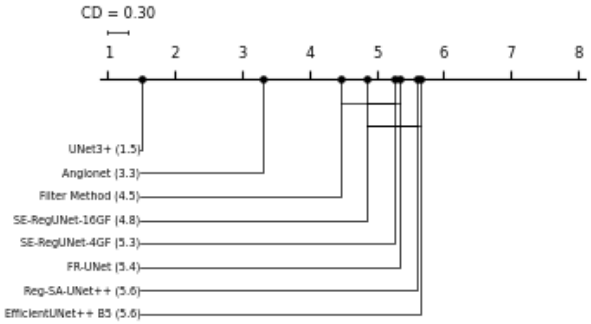

Figure 12: Critical difference diagram for all considered models for the SPEC metric.

The results for the IoU and DSC (Figure 13 - Figure 14) metrics are almost identical, so they will be described collectively. Within these two metrics, four groups of models were formed, which present identical qualitative results of the methods' operation. The group showing the worst results was the group consisting of the UNet3+ network and the filter method. The group consisting of the AngioNet and Reg-SA-UNet++ networks was characterized by better quality of inference. Undoubtedly, the best results were shown by the FR-UNet model, while the rest of the models were placed between the second group and the FR-UNet model.

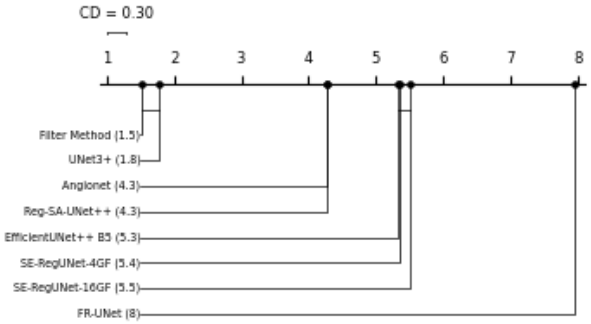

Figure 13: Critical difference diagram for all considered models for the IoU metric.

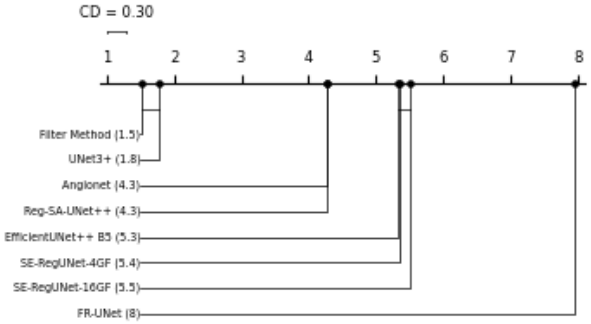

Figure 14: Critical difference diagram for all considered models for the DSC metric.

Taking into account all the obtained results, the FR-UNet model was characterized by the best quality of all considered models and achieved an average accuracy of 97.7%, with the average value of the Dice score metric being 78.2%, which indicates that the model is able to generate a signal that is almost 80% identical to the signal of the ground truth. The observed maximum value of the metric was 87.3%, and the minimum was 61.3%. This is a large discrepancy and indicates that not every signal is equally easy to process.

The AngioNet, EfficientUNet++ B5, Reg-SA-UNet++ models and two variants of the SE-RegUNet model achieved the Dice score metric value at a similar level of about 60%, respectively for AngioNet - 59.1%, EfficientUNet++ B5 - 64.8%, Reg-SA-UNet++ - 60%, SE-RegUNet-16GF - 66% and SE-RegUNet-4GF - 62.7%. This shows that despite the differences and improvements introduced in these convolutional network architectures, the results do not increase significantly, which may indicate their limitations and the need to search for new solutions. In terms of the Dice score metric, the filter method achieved very poor results at an average level of 25.2%, which completely disqualifies this method in practical applications.

The UNet3+ model had the lowest accuracy, achieving an average result of 88%. A case was observed in which the Dice score value was 74.4%, but also a case was observed for which none of the pixels received the correct semantic class through prediction, i.e. achieved Dice score value was equal to zero.

6. Conclusions

In this paper, a study was conducted on the comparison of the quality of models used for semantic segmentation of the coronary vessel structure based on source coronary angiographic images. The selected models and machine learning algorithms and one filter method showed significant differences in the quality of segmentation mask predictions. For each considered metric, the Friedman rank test and the Nemenyi post-hoc test were performed, based on which it can be concluded that the model showing the best quality was the FR-UNet model, while the model with clearly the worst results was the UNet3+ model. The remaining models, depending on the metric, were placed in different places in the hierarchy. It is not possible to indicate an exact hierarchy for all the models considered, due to the ambiguity resulting from the experiment results.

In the future, an interesting consequence of research in this area may be the geometric analysis of the coronary vessel structure and the fusion of vessel geometry and the possibility of building a coronary vessel graph. Studying the mathematical properties of such structures could allow for the development of an objective metric, based on which automatic processing tools and artificial intelligence models would be able to determine its compliance with the reference structure of a healthy person. In the case of sick people, however, a thorough analysis of places in the graph that show irregularities and find this place in the analyzed coronary angiography should be performed, and then the digital image should be analyzed only and exclusively in fragments that show divergent properties compared to a healthy person. This would make it possible to analyze this sensitive fragment of the human body not only in terms of stenoses in arteries and veins, but also to look at anomalies in the geometric structure of the coronary vessels itself, which at the stage of development of the human body may be shaped pathologically. In this field, it is still worth conducting research aimed at better understanding the mathematical properties of the human body, which will help us objectively assess the state of human health in a machine way.

References

[1] The top 10 causes of death, https://www.who.int/news-room/fact-sheets/detail/the-top-10-causes-of-death, [06.01.2025].

[2] A. F. Frangi, W. J. Niessen, K. L. Vincken, M. A. Viergever, Multiscale vessel enhancement filtering, Lecture Notes in Computer Science (including subseries Lecture Notes in Artificial Intelligence and Lecture Notes in Bioinformatics) 1496 (1998) 130–137, https://doi.org/10.1007/BFB0056195.

[3] H. Fazlali, N. Karimi, S. Soroushmehr, S. Samavi, B. Nallamothu, H. Derksen, K. Najarian, Robust catheter identification and tracking in X-ray angiographic sequences, In 2015 37th Annual International Conference of the IEEE Engineering in Medicine and Biology Society (EMBC) (2015) 7901–7904.

[4] M. T. Dehkordi, A. M. D. Hoseini, S. Sadri, H. Soltanianzadeh, Local feature fitting active contour for segmenting vessels in angiograms, IET Computer Vision 8(3) (2014) 161–170, https://doi.org/10.1049/IET-CVI.2013.0083.

[5] B. Felfelian, H. Fazlali, N. Karimi, S. Soroushmehr, S. Samavi, B. Nallamothu, K. Najarían, Vessel segmentation in low contrast X-ray angiogram images, In 2016 IEEE International Conference on Image Processing (ICIP) (2016) 375–379.

[6] A. Hernandez-Vela, C. Gatta, S. Escalera, L. Igual, V. Martin-Yuste, M. Sabate, Accurate coronary centerline extraction, caliber estimation and catheter detection in angiographies, IEEE Transactions on Information Technology in Biomedicine 16(6) (2012) 1332–1340, https://doi.org/10.1109/TITB.2012.2220781.

[7] O. Ronneberger, P. Fisher, T. Brox, U-Net: Convolutional Networks for Biomedical Image Segmentation, IEEE Access 9 (2015) 16591–16603, https://doi.org/10.1007/978-3-319-24574-4_28.

[8] H. Huang, L. Lin, R. Tong, H. Hu, Q. Zhang, Y. Iwamoto, UNet 3+: A Full-Scale Connected UNet for Medical Image Segmentation, In International Conference on Acoustics, Speech, and Signal Processing (ICASSP) IEEE (2020) 1055–1059.

[9] Z. Zhou, M. Rahman Siddiquee, N. Tajbakhsh, J. Liang, Unet++: A nested u-net architecture for medical image segmentation, In: Stoyanov, D., *et al.* Deep Learning in Medical Image Analysis and Multimodal Learning for Clinical Decision Support. DLMIA ML-CDS 2018 2018. Lecture Notes in Computer Science(), Springer 11045 (2018) 3–11, https://doi.org/10.1007/978-3-030-00889-5_1.

[10] W. Liu, H. Yang, T. Tian, Z. Cao, X. Pan, W. Xu, Y. Jin, F. Gao, Full-Resolution Network and Dual-Threshold Iteration for Retinal Vessel and Coronary Angiograph Segmentation, IEEE Journal of Biomedical and Health Informatics 26(9) (2022) 4623–4634, https://doi.org/10.1109/JBHI.2022.3188710.

[11] I. Radosavovic, R. P. Kosaraju, R. Girshick, K. He, P. Dollár, Designing Network Design Spaces, In Conference on Computer Vision and Pattern Recognition (CVPR) IEEE/CVF (2020) 10425–10433.

[12] C. Niu, O. Gao, W. Lu, W. Liu, and T. Lai, Reg-SA-UNet++: A Lightweight Landslide Detection Network Based on Single-Temporal Images Captured Postlandslide, IEEE Journal of Selected Topics in Applied Earth Observations and Remote Sensing 15 (2022) 9746–9759, https://doi.org/10.1109/JSTARS.2022.3219897.

[13] S. Chang, C. Lin, W. Wang, K. Hsu, Y. Wu, C. Liu, Y. Fann, Optimizing ensemble U-Net architectures for robust coronary vessel segmentation in angiographic images, Scientific Reports 14(1) (2024) 1–11, https://doi.org/10.1038/s41598-024-57198-5.

[14] K. Iyer, C. Najarian, A. Fattah, C. Arthurs, S. Soroushmehr, V. Subban, M. Sankardas, R. Nadakuditi, B. Nallamothu, C. Figueroa, AngioNet: a convolutional neural network for vessel segmentation in X-ray angiography, Scientific Reports 11(1) (2021) 1–13, https://doi.org/10.1038/s41598-021-97355-8.

[15] F. Cervantes-Sanchez, I. Cruz-Aceves, A. Hernandez-Aguirre, M. A. Hernandez-Gonzalez, S. E. Solorio-Meza, Automatic segmentation of coronary arteries in X-ray angiograms using multiscale analysis and artificial neural networks, Applied Sciences (Switzerland) 9(24) (2019) 5507, https://doi.org/10.3390/app9245507.

[16] C. Zhao, A. Vij, S. Malhotra, J. Tang, H. Tang, D. Pienta, Z. Xu, W. Zhou, Automatic extraction and stenosis evaluation of coronary arteries in invasive coronary angiograms, Computers in Biology and Medicine 136 (2021) 104667, https://doi.org/10.1016/J.COMPBIOMED.2021.104667

[17] M. N. Menezes, J. Lourenço-Silva, B. Silva, T. Rodrigues, A. R. G. Francisco, P. C. Ferreira, A. L. Oliveira, F. J. Pinto, Development of deep learning segmentation models for coronary X-ray angiography: Quality assessment by a new global segmentation score and compari-son with human performance, Revista Portuguesa de Cardiologia 41(12) (2022) 1011–1021, https://doi.org/10.1016/J.REPC.2022.04.001

[18] OpenCV - Open Computer Vision Library, https://opencv.org/, [04.05.2025]

[19] Z. Wang, A. C. Bovik, H. R. Sheikh, E. P. Simoncelli, Image quality assessment: From error visibility to structural similarity, IEEE Transactions on Image Processing 13(4) (2004) 600–612, https://doi.org/10.1109%2FTIP.2003.819861

[20] FR-UNet: Full-Resolution Network official repository, https://github.com/lseventeen/FR-UNet, [02.05.2025].

[21] KurtLin Coronary Angio Segment official repository, https://huggingface.co/spaces/KurtLin/CoronaryAngioSegment_Rescale/tree/main, [02.05.2025].

[22] M. Friedman, A Comparison of Alternative Tests of Significance for the Problem of m Rankings, 11(1) (1940) 86–92, https://doi.org/10.1214/AOMS/1177731944.

[23] P. B. Nemenyi, Distribution-Free Multiple Comparisons, PhD dissertation, Princeton University, 1963